RILEM Bookseries

Hans Beushausen · Joanitta Ndawula · Mark Alexander · Frank Dehn · Pilate Moyo *Editors*

Proceedings of the 7th International Conference on Concrete Repair, Rehabilitation and Retrofitting

ICCRRR 2024

Springer

Assessment of SFRC Slab-on-Piles Through In-Situ Load Testing

Cosmin Popescu[1,2(✉)] and Björn Täljsten[1,3]

[1] Invator AB, 181 46 Lidingö, Sweden
cosmin.popescu@invator.se
[2] SINTEF Narvik, 8517 Narvik, Norway
[3] Luleå University of Technology, 971 87 Luleå, Sweden

Abstract. Demonstrating the performance of a structural component is typically accomplished through calculations based on engineering models. However, advancements in material science have enabled the use of new materials in the construction industry. One example is fibre-reinforced concrete, which consists of concrete with short, discontinuous fibres dispersed throughout its volume to enhance performance under service limit states. The absence of conventional reinforcement can affect ductility and load capacity, making calculations alone insufficient to demonstrate the performance of these elements. Therefore, load-testing programs need to be developed. This paper reports and discusses the results of a full-scale test on a fibre-reinforced concrete multi-span slab-on-piles. The development of the test program, including the loading setup to achieve failure loads, is presented. The slab's performance is evaluated in terms of deflections and crack widths at various loading intervals corresponding to both service limit states and ultimate limit states.

Keywords: Full-Scale Test · SFRC · Slab-on-Piles

1 Introduction

Fiber-reinforced concrete (FRC), particularly steel fiber-reinforced concrete (SFRC), is increasingly used for crack control in concrete structures, thereby enhancing their serviceability. The performance of SFRC depends on fiber characteristics such as shape, aspect ratio, steel properties, and dosage, which collectively influence the post-peak tensile strength of the concrete.

SFRC can be used alongside reinforcing bars primarily to control cracks within acceptable limits [1]. Alternatively, using SFRC as the sole reinforcement is becoming popular due to its constructability and economic benefits [1, 2]. Typical applications of SFRC as sole reinforcement include slabs-on-grade and tunnel linings [3]. Slabs-on-grade rely on the ground for efficient load transfer. To address poor ground capacity, piles can be introduced to transfer loads to the bedrock, creating a slab-on-piles structure. For a slab-on-piles, it is assumed that the ground provides no support other than as in-situ

H. Beushausen et al. (Eds.): ICCRRR 2024, 59, pp. 88–98, 2025.
https://doi.org/10.1007/978-3-031-75507-1_9

formwork, so the design relies on methods applicable to suspended slabs. Designers often use yield-line theory, which requires adequate ductility to assume plastic behavior.

The plastic behavior of a slab depends on its ductility. The ductility of SFRC slabs-on-ground is not yet well understood. Eliminating conventional reinforcement in a slab-on-piles structure often results in thicker slabs for large spans and/or high distributed loads [4]. One way to achieve thinner slabs is by considering the arch effect in multi-span slabs, an aspect recently recognized in studies. Although the use of SFRC slabs-on-piles without conventional reinforcement is gaining popularity, consensus on design methods has not been established. To contribute to the understanding of such structures, evaluating their performance through full-scale in-situ load testing is necessary. This paper presents the development of a test program, including the loading setup to achieve the failure loads of a full-scale slab-on-piles.

2 Slab Under Test: Geometric Features and Material Properties

The tested slab is designed to replicate a section of a large slab-on-piles from a warehouse (Fig. 1). For practical reasons, the slab size has been limited to fewer bays compared to the original structure, resulting in a 5 × 4 bay configuration. Each pile has a diameter of 700 mm and supports a 250-mm-thick SFRC slab. The piles transfer vertical loads to isolated foundations cast on a well-packed gravel layer. The distance between the piles is 3.8 m.

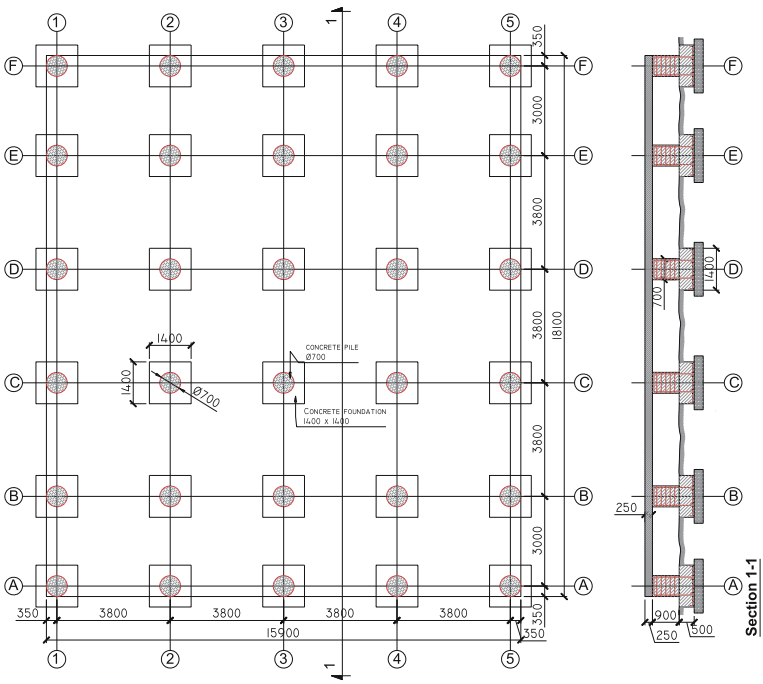

Fig. 1. General dimension of the tested slab-on-piles.

The material properties used for constructing the slab matched those specified in the original documentation. This included the type and dosage of fibers and the concrete strength. ArcelorMittal (HE + 1/60) fibers were used, with the fiber dosage measured on site, averaging approximately 48 kg/m^3. The concrete compressive strength was determined from cubes made during casting and tested at 28 days, as well as from cores extracted from the slab and tested at 43 days. The values obtained were approximately 35.3 ± 3.16 MPa and 43.0 ± 2.95 MPa, respectively.

3 Test Program

3.1 Loading Arrangement

The slab testing involved performance evaluation under both service and ultimate limit states as outlined by the Eurocode. A distributed load with a characteristic value of 40 kN/m^2 was applied to the slab. Due to practical constraints, only a limited area of the slab was loaded. This area was chosen through an iterative process using finite element (FE) analysis, which considered multiple loading arrangements to achieve maximum bending moments in the field and over supports simultaneously. The final loading arrangement is depicted in Fig. 2 (hatched area).

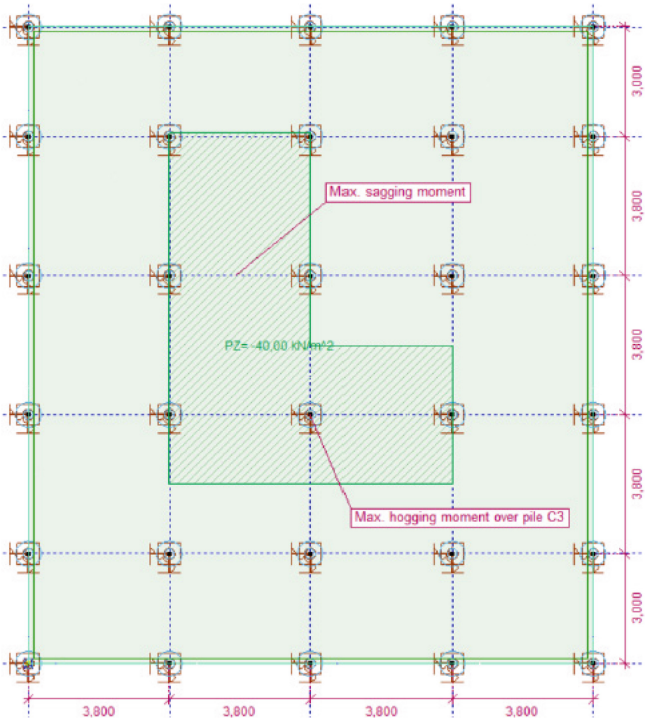

Fig. 2. FE model: geometry, load configuration and areas of maximum positive and negative bending moments.

The slab was loaded in five distinct sequences. The first sequence corresponded to the service limit state with a safety factor of 1.0. The second to fourth sequences corresponded to the ultimate limit state, each representing a different safety class. When using the partial coefficient method according to SS-EN 1990 for the ultimate limit state, the safety class for a construction part is considered using the partial coefficient γd as follows: safety class 1 with $\gamma_d = 0.83$, safety class 2 with $\gamma_d = 0.91$, and safety class 3 with $\gamma_d = 1.0$. The final sequence was a test to failure. The final loads achieved in each sequence are shown in Table 1.

Table 1. Loads per each sequence.

Sequence	1	2	3	4	5
Own weight, kN/m^2				6.0	
Distributed load, kN/m^2			40		
Safety factor[1)], $\gamma_d \times \gamma_Q$	1.0	1.3	1.365	1.5	
Factored load	40	52	55	60	≈ 80[2)]

[1)] The safety factor = $\gamma_d \times \gamma_Q$; where γ_d is a safety class coefficient and γ_Q – partial safety factor for variable loads; $\gamma_Q = 1.0$ in SLS and $\gamma_Q = 1.4$ in ULS

[2)] Total load applied on the slab at failure excluding its own weight

The load was applied according to a predetermined schedule, with increments of 10 kN/m^2 added to the slab until the intended load level was reached. The load was then maintained for up to 7 days before being removed, as shown in Fig. 3. The testing procedure was conceptually similar for all load tests, with a few differences. For instance, in load sequence 3, the load was maintained overnight instead of 7 days and then continued up to 60 kN/m^2 (load sequence 4). In load sequence 5, the loads were gradually applied until failure was achieved.

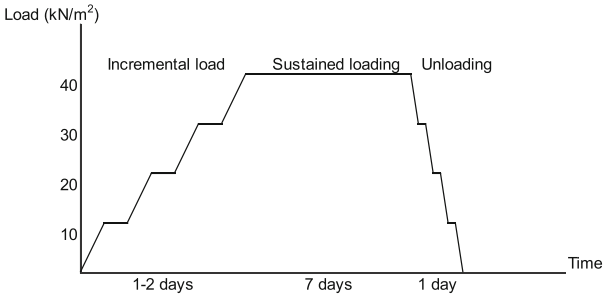

Fig. 3. Modified load sequence based on ACI 437.2-13.

To simulate distributed loads as accurately as possible, the load material used was fines (steel slag, a by-product of steelmaking) with a density of 3500 kg/m^3, as shown in Fig. 4a. This material was chosen due to its high density and ability to conform to the

surface. Additionally, the bags do not interlock, and the magnetite gravel molds itself, preventing a bridging effect. This ensures that the intended load height is lower while maintaining an evenly distributed load, as illustrated in Fig. 4b. The load was applied using large bags with a bottom area of 0.9 × 0.9 m. Each bag was individually weighed, and the weight was marked on the bag.

(a) (b)

Fig. 4. Loaded slab: (a) loading material; and (b) placement of the loads on the slab.

3.2 Instrumentation

To evaluate the slab's behavior, a comprehensive measurement program was designed. This section summarizes the instrumentation used to monitor changes in various parameters during the slab tests. The following measurements were recorded:

- **Deformations in the field**: Measured in two directions throughout the test (both loading and unloading) using 13 LVDTs mounted on a stiff frame attached to the piles.
- **Curvature**: Indirectly measured by assessing deformations.
- **Crack propagation over supports and in the field**: Monitored through visual inspection, crack width measurements with a crack microscope, and crack depth using ultrasound Pundit Lab.
- **Concrete strains**: Crack propagation over supports and in the field monitored using Luna OSF ODiSi 6000 Fiber Optic equipment.
- **Crack propagation**: Monitored in a limited area using digital image correlation.
- **Crack opening**: Measured after the first dominant crack (bottom of the slab) with micro measurement MM HS 10.
- **Temperature**: Recorded both below and above the slab.
- **Loading**: Monitored manually by weighing and using pressure film (Fujifilm printing film).
- **Surveillance cameras**: Used to monitor the full-scale test (Bascom Pro bullet camera) and to observe crack propagation and slab failure (Axis F1015 placed under the slab).

The FE model was used as a rough guide to position the instrumentation where maximum responses were expected. The sensor locations for monitoring the slab's

response during load testing are shown in Fig. 5. Due to space limitations, only selected measurements are reported.

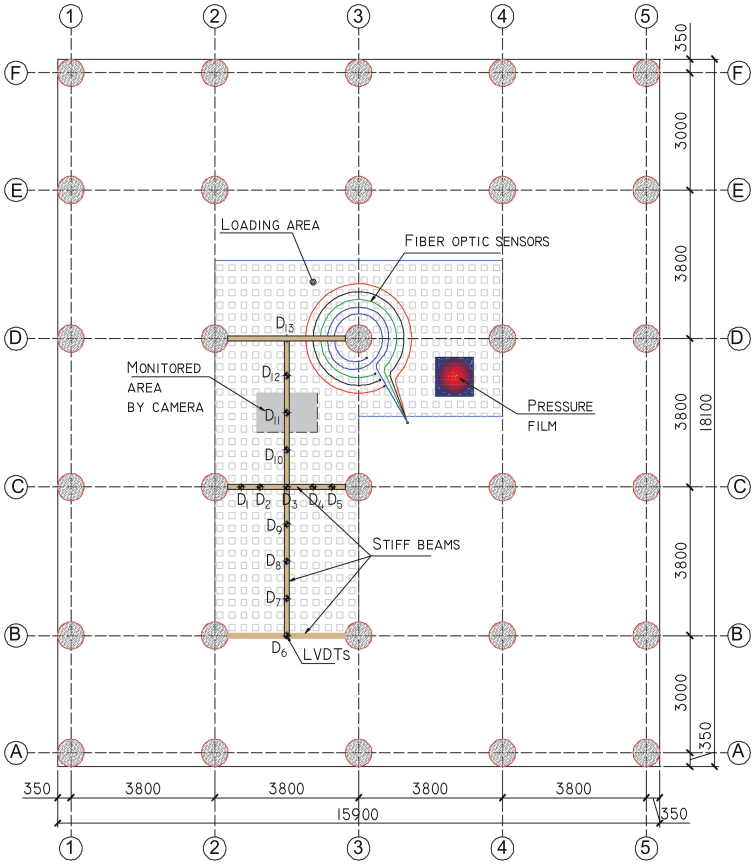

Fig. 5. Instrumentation plan.

4 Test Results

In this section, the test results are presented in terms of deflections, crack patterns, and crack widths at selected load levels.

Deflection at the serviceability limit state (SLS) of 40 kN/m^2 is shown in Fig. 6. Distinct phases can be observed. In Phase 1, at approximately 2 mm deformation, cracking occurs, rapidly increasing the deformation to around 5.0 mm. After about 4 days, the deformation levels off, reaching a maximum of about 6.5 mm after 7 days. The largest deformation was observed at LVDT sensor D8. Upon unloading, residual deformation was approximately 3.17 mm, reducing to 3.04 mm after a further 3 days.

Figure 7 illustrates the crack pattern at SLS. Mapping was done visually by hand on the lower side and with drone support on the upper side. Regions where crack widths and depths were investigated are shown in Fig. 7. On the bottom, a thin crack was noted, with widths ranging from 0.11 mm in region 8 to 0.41 mm in regions 3 and 10. On the top surface, a small, barely visible crack was observed above pile C3, with a width of about 0.08 mm. The crack widths were measured at the end of the 7-day sustained load period, just before unloading.

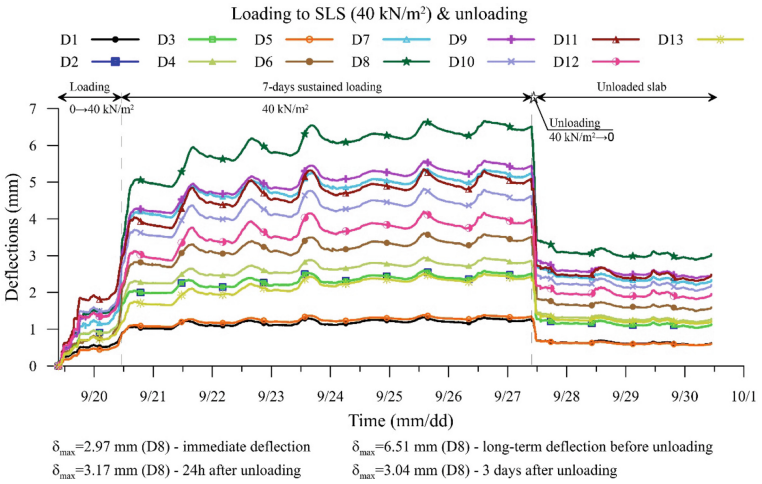

Fig. 6. Deflection under the serviceability limit state, SLS – 40 kN/m^2

Deflection at the ultimate limit state (ULS) of 60 kN/m^2 is shown in Fig. 8. Deformation increased to approximately 18.0 mm when the load reached 55 kN/m^2, which was then maintained for a day before being increased to 60 kN/m^2. At the ULS load level, deformations increased to approximately 19 mm. After the load was applied for less than a week, the deformation reached approximately 22.1 mm. The deformation leveled off towards the end of the loading sequence.

Although cracking is relevant for the service limit state, it was also monitored at the ULS. Once the main crack appeared at the SLS, an LVDT was mounted over the crack to track its progression. At the ULS, the crack grew to approximately 2.20 mm for crack 1 and approximately 2.25 mm for crack 2. The crack pattern developed throughout all loading stages is shown in Fig. 9.

The final loading sequence aims to determine the ultimate load-carrying capacity of the slab. Figure 10 illustrates the deformation diagram for all load sequences, including the load leading to failure. Observing this diagram, we can identify two stabilization phases of the plate. The first occurs at the service load of 40 kN/m^2, where the plate exhibits very stable behavior after initial cracking. The second stabilization phase occurs at approximately 55–60 kN/m^2, where the behavior remains stable, with a plateau of around 20 mm deformation along the long direction of the plate. At the point of failure (Fig. 11), we observe an increase in deformation without a corresponding increase in

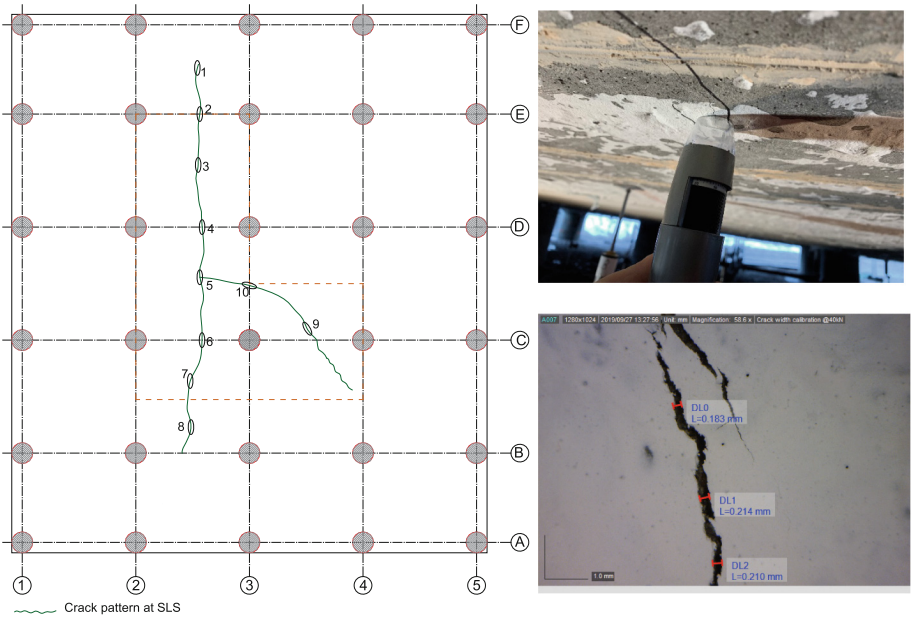

Fig. 7. Crack pattern and crack widths after loading at SLS – 40 kN/m^2

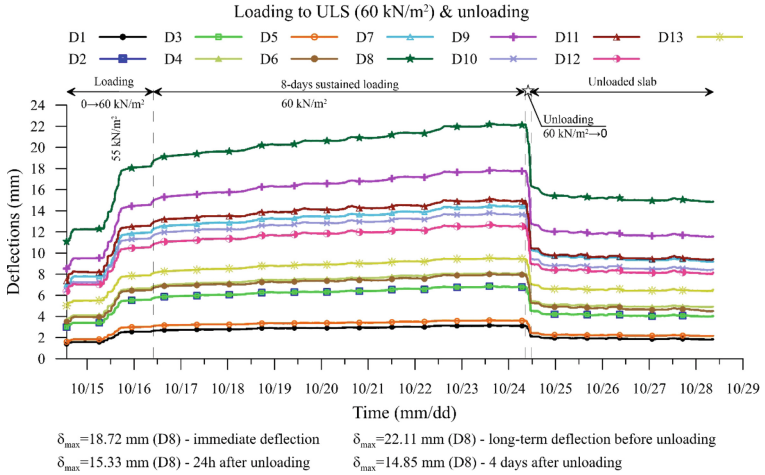

Fig. 8. Deflection under the ultimate limit state, ULS – 60 kN/m^2

load. The measurement ceases at approximately 55 mm relative to the original position due to the rapid failure process, which was load-controlled. As a result, no further deformations are recorded as the sensors were destroyed by the failed slab. The slab failed at 77.8 kN/m^2, including its own weight of approximately 6 kN/m^2, resulting in a total failure load of about 83.4 kN/m^2.

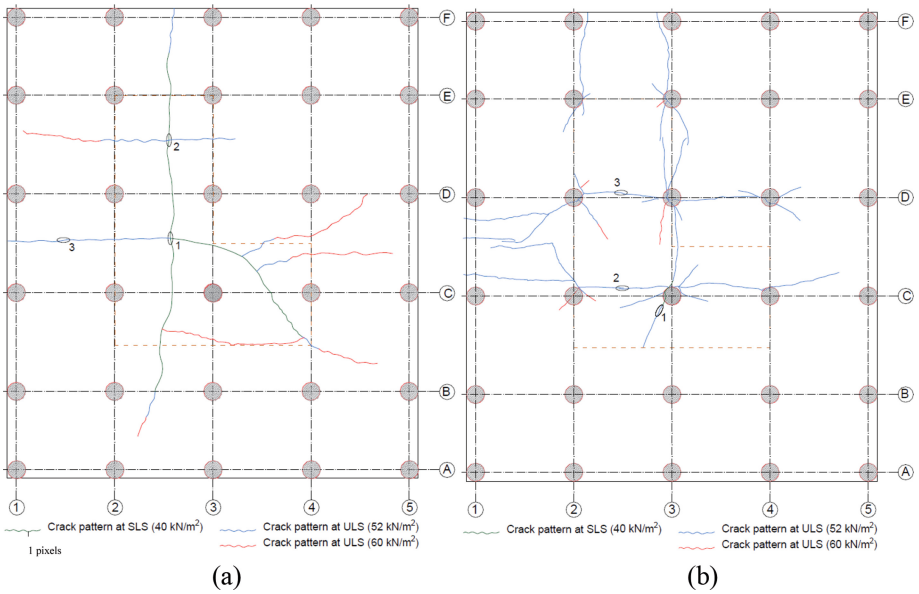

Fig. 9. Crack pattern after each loading sequence: (a) bottom surface; and (b) top surface.

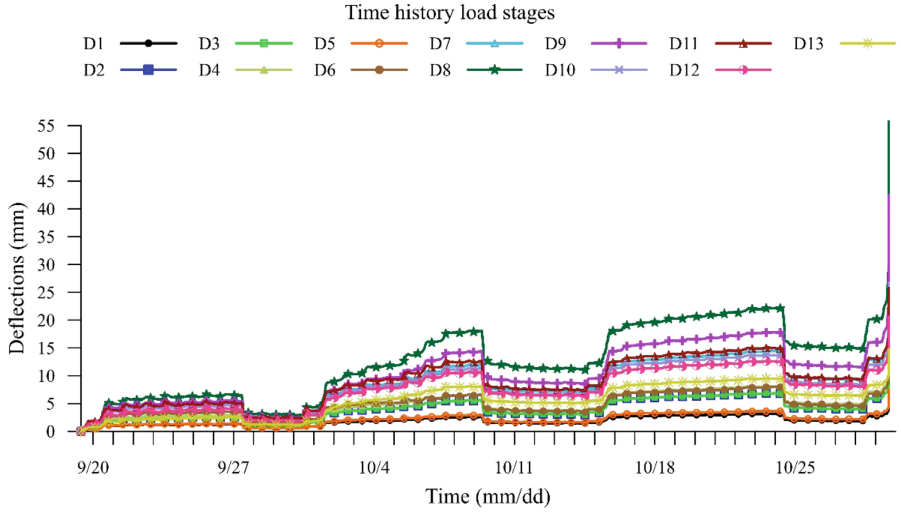

Fig. 10. Deflection during all load sequences, from SLS to ULS and up to failure, 40 – 77.8 kN/m^2

5 Conclusions

The conducted testing is extensive and distinguished by the size of the loaded slab and the level of applied load, rendering it unique. The primary aim of the test has been to assess the load-bearing capacity and behavior of the SFRC pile-supported slab under

Fig. 11. Photo after failure – before and after removal of the loading bags.

both serviceability and ultimate limit states. Additionally, the investigation seeks to understand the safety margins that the slab possesses against the ultimate limit state.

In the serviceability limit state (SLS), a crack width of approximately 0.41 mm was measured. The requirements stipulated for the floor in the SLS are 0.6 mm, thus indicating that the slab meets the SLS criteria. The largest measured deformation is approximately 6.51 mm, satisfying the requirements (L/500 = 7.6 mm) established for the floor in the service limit state.

Under all loads, ranging from 52 kN/m^2 to 60 kN/m^2 in the ultimate limit state (ULS), the slab demonstrates stable behavior. Each load sequence within the ULS experiences a phase of increased deformation, which levels off towards the end of the period. Analysis of the slab's behavior under loads up to 60 kN/m^2 suggests that there is no risk of damage to property or individuals.

Furthermore, the ultimate load achieved by the slab at failure significantly exceeded the design load at ULS, by almost 30%. It's noteworthy that the load underwent cyclic loading and unloading, and the load in the ULS was sustained for an extended period, which contrasts with the typical short-term load in reality. Moreover, the test was conducted at ambient temperature, impacting the testing process; increased temperature led to raised deformations and cracking, which did not reverse upon temperature decrease due to the constant load. Hence, the temperature effect acts as an additional load case, unusual for traditional warehouses. Nonetheless, the slab demonstrates robust behavior with minimal deformations and cracking in the SLS, and controlled deformations and cracking in the ULS.

References

1. Hedebratt, J., Silfwerbrand, J.: Full-scale test of a pile supported steel fibre concrete slab. Mater. Struct. **47**(4), 647–666 (2014). https://doi.org/10.1617/s11527-013-0086-5
2. Destrée X., Mandl J.: Steel Fibre Only Reinforced Concrete in Free Suspended Elevated Slabs: Case Studies, Design Assisted by Testing Route, Comparison to the Latest SFRC Standard Documents, Tailor Made Concrete Structures, Taylor & Francis, London, UK (2008)
3. Jansson A., Gylltoft K., Löfgren I.: Design methods for fibre-reinforced concrete: a state-of-the-art review. Nordic Concrete Research, Publication No. 38. 31-46 (2008)

4. Hedebratt J., Silfwerbrand J.: An innovative approach to the design of pile supported SFRC slabs. In: di Prisco, M., Felicetti, R., Plizzari, G.A. (eds.) 6th RILEM Symposium on Fibre-Reinforced Concretes (FRC), pp. 945–954 (2004)